iScience

CellPress
OPEN ACCESS

Article

Synaptotagmin 2 is ectopically overexpressed in excitatory presynapses of a widely used CaMKIIα-Cre mouse line

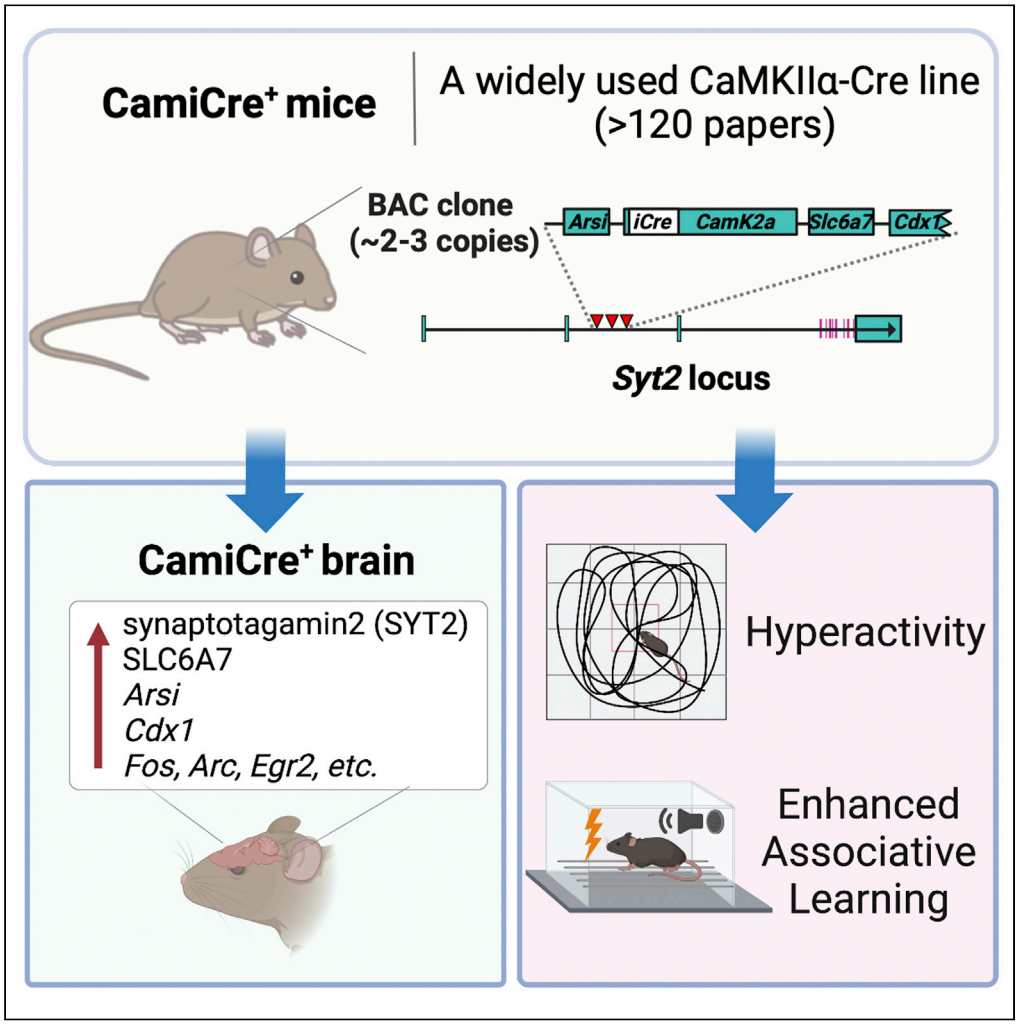

Ken Matsuura, Haytham M.A. Mohamed, Mohieldin M.M. Youssef, Yutaka Yoshida, Tadashi Yamamoto

ken.matsuura@oist.jp (K.M.)
tadashi.yamamoto@oist.jp (T.Y.)

Highlights

CamiCre+ mice show the ectopic overexpression of SYT2 in excitatory presynapses

CamiCre+ mice show the ectopic overexpression of SLC6A7 in hippocampal mossy fibers

CamiCre+ mice show hyperactivity and enhanced associative learning

Multiple copies of bacterial artificial chromosome (BAC) transgenes are integrated into the *Syt2* locus

Matsuura et al., iScience *25*, 104692
August 19, 2022
https://doi.org/10.1016/j.isci.2022.104692

iScience

CellPress
OPEN ACCESS

Article

Synaptotagmin 2 is ectopically overexpressed in excitatory presynapses of a widely used CaMKIIα-Cre mouse line

Ken Matsuura,[1,3,6,*] Haytham M.A. Mohamed,[1,2] Mohieldin M.M. Youssef,[1] Yutaka Yoshida,[3,4,5] and Tadashi Yamamoto[1,*]

SUMMARY

The CaMKIIα-Cre mouse lines, possibly the most used Cre lines in neuroscience, have resulted in over 800 articles to date. Here, we demonstrate that the second most widely used CaMKIIα-Cre line, Tg(Camk2a-cre)2Gsc (or CamiCre), shows ectopic overexpression of synaptotagmin 2, the most efficient Ca^{2+} sensor for fast synchronous neurotransmitter release, in excitatory presynapses of Cre^{+} brains. Moreover, the upregulation of immediate-early genes and genes incorporated in bacterial artificial chromosome (BAC) transgenes, such as L-proline transporter *Slc6a7*, was found in Cre^{+} hippocampus. The copy number and integration site of the transgene are suggested to have caused the aberrant gene expression in Cre^{+} brains. Most importantly, CamiCre^{+} mice showed functional phenotypes, such as hyperactivity and enhanced associative learning, suggesting that neural activities are affected. These unexpected results suggest difficulties in interpreting results from studies using the CamiCre line and raise a warning of potential pitfalls in using Cre driver lines in general.

INTRODUCTION

The Cre-loxP system is one of the most powerful and commonly used techniques in neurogenetics, as well as in diverse biomedical studies, ranging from spatial and/or temporal gene-knockout (KO)s/knockin (KI)s and neural pathway tracing, to optogenetics (Branda and Dymecki, 2004; Daigle et al., 2018; Gerfen et al., 2013). The CaMKIIα-Cre mouse was the first Cre driver line in neurogenetics that showed successful recombination of DNA between two palindromic *loxP* sites inserted in critical positions of a gene of interest by the bacteriophage DNA-recombinase Cre to generate conditional gene-KO in principle neurons of mouse forebrain (Tsien et al., 1996a, 1996b). There are currently 37 CaMKIIα-Cre lines available, with 31 of them used in one or more articles (Figure S1A) according to the Mouse Genome Informatics (MGI) database (Bult et al., 2019) . These mouse lines are used in various studies addressing gene functions in electrophysiology, learning and memory, circadian rhythm, metabolism regulation, neuropsychiatric disease models, and so forth, in over 800 publications to date (Figure S1A).

CamiCre is the second most widely used line next to the original CaMKIIα-Cre line, Tg(Camk2a-cre)T29-1Stl (T29-1) (Tsien et al., 1996a, 1996b), and has been used in at least 126 articles since its first appearance in 2001 (Casanova et al., 2001) (Figure S1A), many of them in high impact journals (http://www.informatics.jax.org/reference/allele/MGI:2181426?typeFilter=Literature#myDataTable=results%3D25%26startIndex%3D0%26sort%3Dyear%26dir%3Ddesc%26typeFilter%3DLiterature). The main feature of CamiCre mice is the incorporation of bacterial artificial chromosome (BAC) technology, which utilizes a large genomic region of ~150 kilobases (kb). Compared to a strategy using a smaller promoter region (~10 kb) as in the original T29-1 (Tsien et al., 1996a), it is postulated to improve the fidelity of expression of Cre recombinase under the control of CaMKIIα regulatory sequences, as BACs contain most, if not all required regulatory elements (Casanova et al., 2001; Gong et al., 2007; Heintz, 2001). Another feature is the use of improved Cre (iCre) to maximize Cre expression and activity (Branda and Dymecki, 2004; Casanova et al., 2001; Shimshek et al., 2002). Expression of Cre is mainly restricted to excitatory principal neurons in the forebrain, but is also enriched in the suprachiasmatic nucleus in the hypothalamus, which makes it a valuable tool for

[1]Cell Signal Unit, Okinawa Institute of Science and Technology Graduate University, Onna-son 904-0495, Japan

[2]Division of Genetics, Department of Cancer Biology, The Institute of Medical Science, The University of Tokyo, 4-6-1, Shirokanedai, Minato-ku, Tokyo 108-8639, Japan

[3]Neural Circuit Unit, Okinawa Institute of Science and Technology Graduate University, Onna-son 904-0495, Japan

[4]Burke Neurological Institute, White Plains, NY 10605, USA

[5]Brain and Mind Research Institute, Weill Cornell Medicine, New York, NY 10065, USA

[6]Lead contact

*Correspondence: ken.matsuura@oist.jp (K.M.), tadashi.yamamoto@oist.jp (T.Y.)

https://doi.org/10.1016/j.isci.2022.104692

research in circadian rhythm and/or regulation of metabolism (Cedernaes et al., 2019; Godinho-Silva et al., 2019).

Synaptotagmin 2 (Syt2) is one of the three synaptotagmins (Syt1, 2, and 9) that act as Ca^{2+} sensors for fast synchronous neurotransmitter release from presynaptic terminals. Ca^{2+} binding to Syt1, 2, or 9 induces their interaction with the soluble NSF attachment protein receptor (SNARE) complexes, thereby displacing complexins from assembled SNARE complexes to trigger neurotransmitter release (Chen et al., 2017; Xu et al., 2007). These three synaptotagmins form a hierarchy of Ca^{2+} sensors with distinct properties, with Syt2 being the fastest isoform (30% faster than Syt1), and Syt9, being the slowest (Xu et al., 2007). Syt2 also triggers a release with shorter latency and higher temporal precision and mediates faster vesicle pool replenishment than Syt1 (Chen et al., 2017). In the mouse forebrain, Syt1 and Syt2 have complementary expression patterns and are localized predominantly to different subsets of synapses (Fox and Sanes, 2007). Syt2 is selectively expressed in inhibitory neurons in this region and preferentially in large axosomatic synapses (Fox and Sanes, 2007; Pang et al., 2006). It is postulated that these different expression patterns support firing properties required for different neuronal types, e.g., Syt2 is the only isoform expressed in the calyx synapse, which relies on very fast signaling (Xu et al., 2007).

Here, we show that CamiCre$^+$ mice show ectopic overexpression of Syt2 in excitatory presynapses in the forebrain and functional phenotypes, such as hyperactivity and enhanced learning, which may compromise research using CamiCre mice. These unexpected and problematic phenotypes in CamiCre mice shed light on the importance of better phenotypic characterization of Cre driver lines and the importance of adopting proper controls, including the incorporation of Cre$^+$ controls that are often neglected.

RESULTS AND DISCUSSION

Synaptotagmin 2 is significantly upregulated in excitatory presynapses of CamiCre$^+$ forebrain

In the course of a project utilizing CamiCre mice to generate conditional KO mice for the gene of interest, we noticed the upregulation of Syt2 in both transcriptomic and proteomic analyses of KO brain compared to *Gene*$^{flox/flox}$; CamiCre$^-$ controls. We were initially excited, but as a result of subsequent qPCR and Western blot experiments that included *Gene*$^{+/+}$; CamiCre$^+$ controls, we soon realized that this upregulation was independent of our gene of interest. Therefore, we deemed it would be important for our project and possibly for any research involving CamiCre mice to characterize this Cre driver line in more detail.

Using the original CamiCre line obtained from the European Mouse Mutant Archive (EMMA), which was backcrossed seven times onto a C57BL/6J genetic background, qPCR results confirmed that *Syt2* mRNA was upregulated more than 5-fold in CamiCre$^+$ hippocampus compared to wild-type (WT) littermate (CamiCre$^-$) controls (Figure 1A). This upregulation was likely owing to increased transcriptional activity suggested by significant upregulation of *Syt2* pre-mRNA (Figure 1A). This upregulation was also confirmed at the protein level by Western blotting of lysates from different brain regions (Figure 1B). Syt2 was overexpressed more than 7-fold in the hippocampus and about 3-fold in the olfactory bulb and cerebral cortex. However, no significant upregulation was observed in caudal brain regions, such as the midbrain, cerebellum, or medulla oblongata (Figures 1C and 1D). Syt1 expression was not changed in any brain region analyzed (Figures 1A, S2A, and S2B). As the effect was restricted to the forebrain of CamiCre$^+$ mice, mimicking the CaMKIIα promoter-driven Cre expression pattern, we wondered whether simple Cre expression could affect the expression of Syt2. We analyzed two additional driver lines, the original CaMKIIα-Cre line T29-1, and Emx1$^{tm1(cre)Ito}$, which also express Cre in neurons of the adult forebrain, utilizing the endogenous *Emx1* promoter in a knock-in strategy (Iwasato et al., 2000). For detailed Cre expression strategy and expression patterns, please refer to the MGI database (T29-1: http://www.informatics.jax.org/allele/MGI:2177650?recomRibbon=open#expression; Emx1-Cre: http://www.informatics.jax.org/allele/MGI:1928281#expression). These mice did not show any upregulation of Syt2 in the hippocampus of Cre$^+$ mice in either mRNA (Figure 1A) or protein (Figure 1E) levels. However, as the Cre expression level was much lower in these two lines than in CamiCre (likely owing to the iCre effect), we also adopted adeno-associated virus (AAV)-mediated Cre expression (AAV1-hSyn-Cre) in hippocampal neurons of WT mice to see whether high expression of Cre would affect the Syt2 expression level (Figures 1E and S2C). The results suggested that the simple expression of Cre in neurons, regardless of its amount, does not affect the Syt2 expression level. This was good news, as the results suggested that using the Cre-loxP system in neurons, in general, is not compromised by Syt2 overexpression.

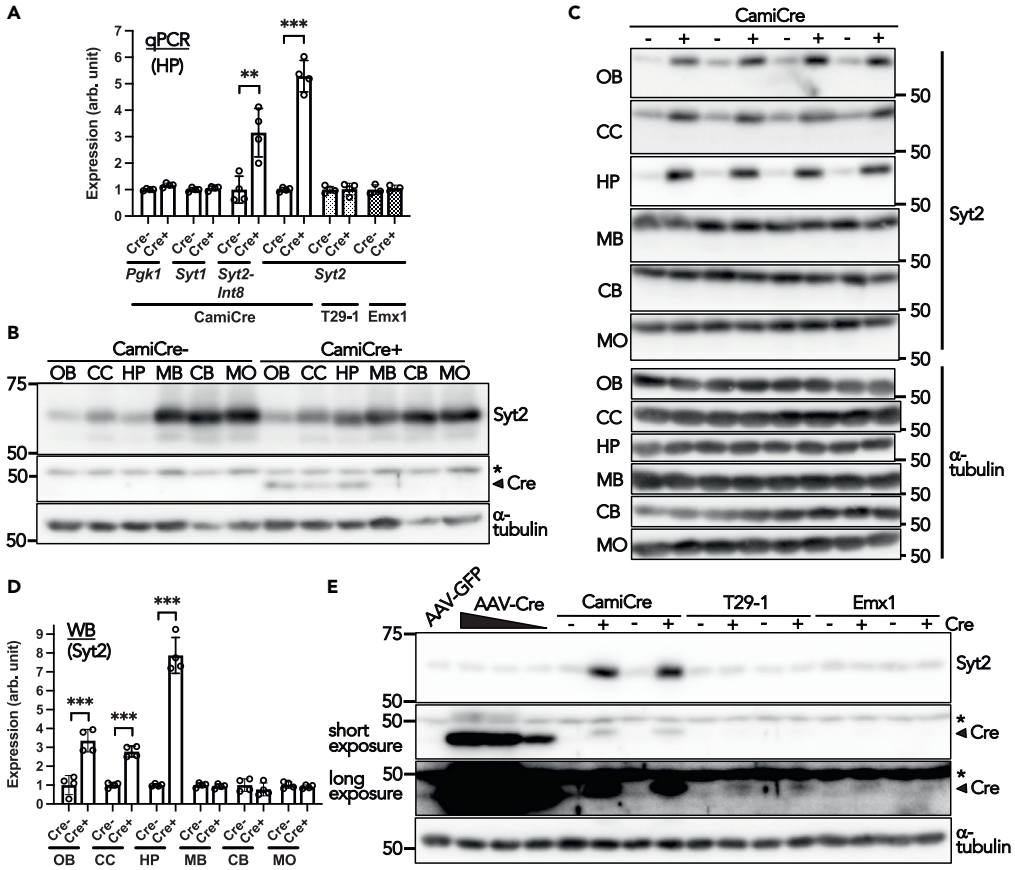

Figure 1. Synaptotagmin 2 is significantly upregulated in CamiCre$^+$ forebrain

(A) qPCR analysis of mRNA expression in the hippocampus in indicated mouse lines. *Syt2-Int8* represents pre-mRNA of *Syt2*. Values were normalized by *Gapdh* expression level and are shown as fold increases against Cre$^-$ controls. *Pgk1* is another housekeeping gene.

(B and C) Western blotting images of different brain regions. CB, cerebellum; CC, cerebral cortex; HP, hippocampus; MB, midbrain; MO, medulla oblongata; OB, olfactory bulb.

(D) Quantification results of C. Values were normalized against α-tubulin expression level and are shown as fold increases against Cre$^-$ controls.

(E) Western blotting images of hippocampal lysates showing Syt2 expression levels in various Cre-expressing methodologies. Viral concentration was diluted 2x in three steps for AAV-hSyn-Cre expression. *, nonspecific band. Mean ± SD is shown. **p < 0.01; ***p < 0.001. N = 4 (biological replicates). Statistical tests were performed using two-tailed, unpaired t-tests. See also Figure S2.

The next question was whether Syt2 overexpression occurs in its native location, the synaptic terminals of inhibitory neurons (Fox and Sanes, 2007; Pang et al., 2006), or in other cell types and/or subcellular structures. Immunostaining of Syt2 in the brains of CamiCre$^+$ mice showed a striking difference from WT controls (Figure 2). Syt2 showed strong uniform staining in the neuropil area of the CamiCre$^+$ hippocampus, compared to much more limited and sporadic staining in the neuropil area of WT controls. Syt2 was also highly expressed in the ventral cortical area of the CamiCre$^+$ brain, such as the amygdala, cortical amygdala, and piriform cortex, where it is little expressed in WT mice (Zhou et al., 2020). High-resolution colocalization analysis using a Confined Displacement Algorithm (Ramirez et al., 2010) in the neuropil region of hippocampal CA1, CA3, and layer 3 of piriform cortex demonstrated significant correlation and colocalization of Syt2 with vesicular glutamate transporter 1 (VGlut1), a glutamatergic presynapse marker (Figures 3A and 3B). Interestingly, this association was also observed in the layer 2/3 region of motor cortex, where Syt2 stains strongly in WT brain at the macroscopic level (Figures 2, 3A, and 3B). Most VGlut1 did not colocalize with Syt2 in WT brains, consistent with the idea that Syt2 is originally localized at synaptic terminals of inhibitory neurons (Figure 3B). The Syt2 staining pattern in axosomatic synapses surrounding pyramidal neurons was similar in CamiCre$^+$ and WT hippocampi (Figure 3A). These results

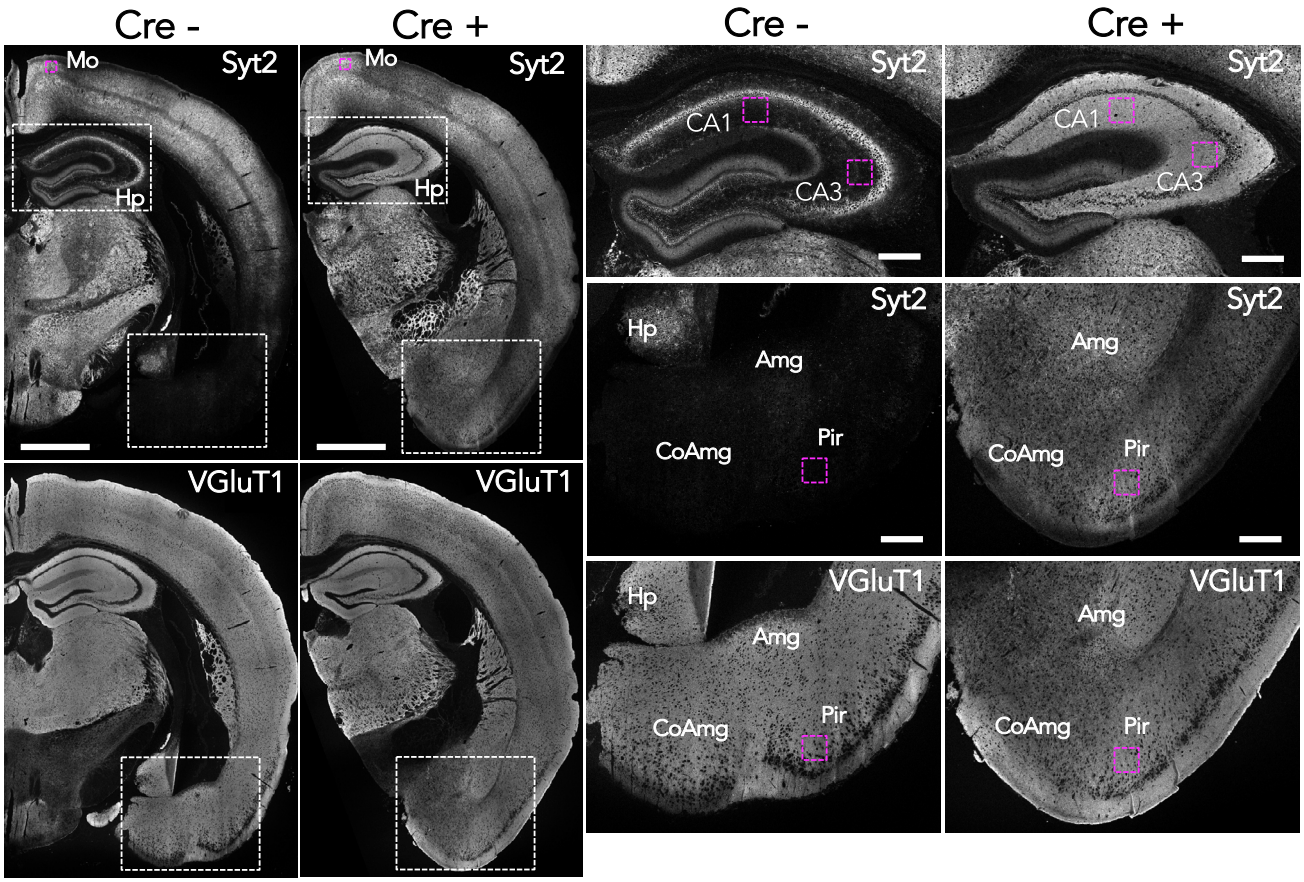

Figure 2. Synaptotagmin 2 is ectopically overexpressed in the hippocampus, amygdala, cortical amygdala, and piriform cortex in CamiCre$^+$ brain

Immunofluorescent images of Syt2 or VGlut1 staining in brains of CamiCre mice. The white dotted boxes in the left panels are magnified in the right panels. The magenta dotted boxes are areas used for colocalization analyses in Figure 3. Amg, amygdala; Co-Amg, cortical amygdala; Hp, Hippocampus; Mo, motor cortex; Pir, piriform cortex. Scale bars: left 1 mm; right 250 μm.

suggested that Syt2 is primarily overexpressed ectopically in presynapses of excitatory neurons in CamiCre$^+$ mice.

The structure of the bacterial artificial chromosome transgene and its genomic integration site are suggested to be the cause of aberrant gene expression in CamiCre$^+$ mice

Using RNA-seq analysis, we further investigated whether there are additional differentially expressed genes in CamiCre$^+$ hippocampus. In addition, we performed parallel analysis on the most widely used T29-1 line to examine whether there are overlaps between the two CaMKIIα-Cre lines. Differential expression (DE) analysis suggested the upregulation of 329 genes in CamiCre$^+$ hippocampus and 247 in T29-1 Cre$^+$ hippocampus. Moreover, 172 and 226 genes were downregulated in CamiCre$^+$ and T29-1 Cre$^+$ hippocampus, respectively (Tables S1 and S2). However, there were no significant overlaps of differentially expressed genes between the two lines (Figure S3A).

Analysis of CamiCre$^+$ hippocampus indicated that 4 genes, including *Syt2*, were overexpressed with remarkably high confidence (Figure S3B and Table S1). Three others, *Slc6a7*, *Arsi*, and *Cdx1*, were found to be located in the genomic region within the arms of the CaMKIIα-iCre BAC transgene used to generate CamiCre mice (Casanova et al., 2001) (Figure 4A). qPCR analyses of hippocampal mRNA gave similar results (Figure 4B). Utilizing genomic qPCR, we next investigated whether these three genes are fully incorporated as transgenes in the CamiCre genome. The results suggested that the majority of BAC clones ranging from upstream of *Arsi* to *Cdx1* were incorporated as at least two copies in the CamiCre$^+$ genome, and possibly three for the region spanning *Arsi* to *Camk2a* (Figure 4C). The BAC clone (RP24-243J21), derived from mouse chromosome 18 (Erdmann et al., 2007), lacks exon 1 of *Cdx1*, which covers 55% of its coding sequence (Figure 4A).

A

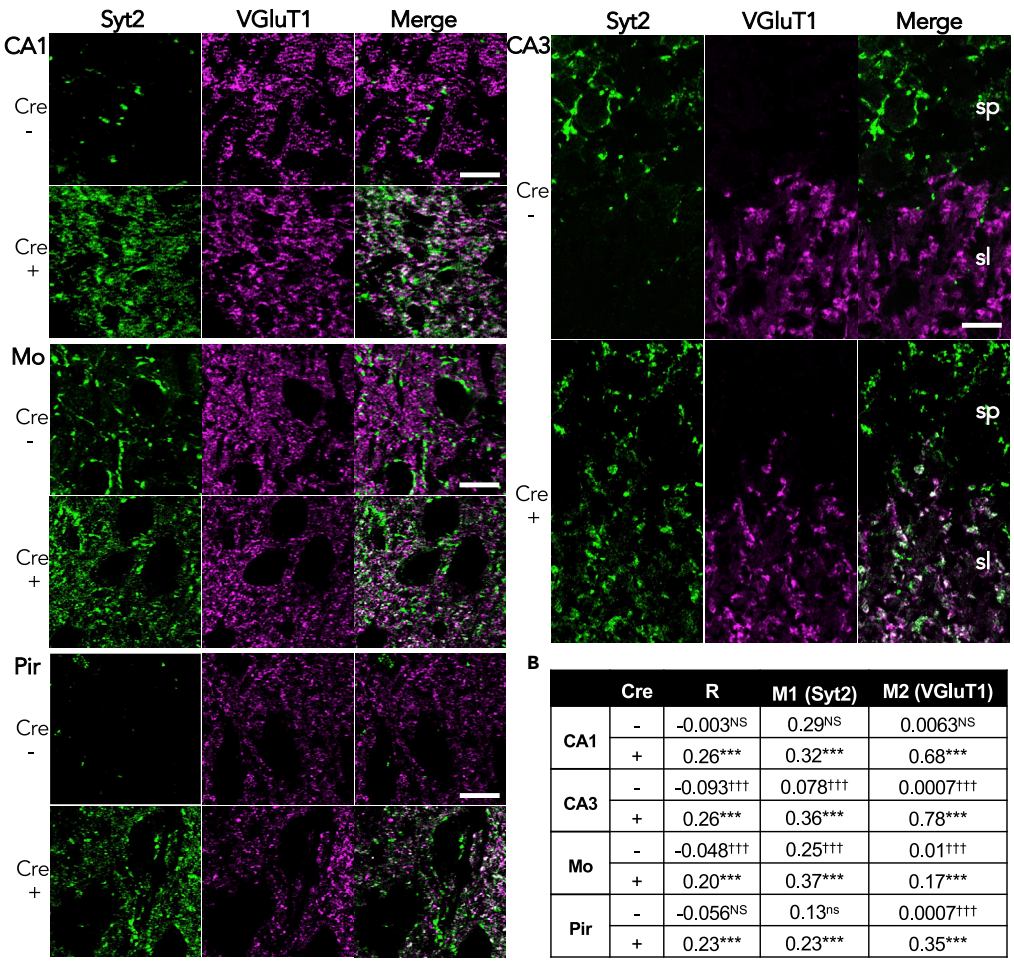

B

	Cre	R	M1 (Syt2)	M2 (VGluT1)
CA1	-	-0.003^{NS}	0.29^{NS}	0.0063^{NS}
	+	0.26***	0.32***	0.68***
CA3	-	-0.093†††	0.078†††	0.0007†††
	+	0.26***	0.36***	0.78***
Mo	-	-0.048†††	0.25†††	0.01†††
	+	0.20***	0.37***	0.17***
Pir	-	-0.056^{NS}	0.13^{ns}	0.0007†††
	+	0.23***	0.23***	0.35***

Figure 3. Synaptotagmin 2 is ectopically overexpressed in excitatory presynapses of CamiCre^{+} cerebrum

(A) Representative high-resolution immunofluorescence images from corresponding areas indicated by magenta dotted boxes in Figure 2 sp, stratum pyramidale; sl, stratum lucidum.

(B) Results from colocalization analyses on a total of 6.3 × 10^4 μm^2 per region. Ectopically expressed Syt2 showed significant colocalization with VGlut1 in CamiCre^{+} brain. R, Pearson correlation coefficient; M1 and M2, Manders coefficient. NS, not significant; ***p < 0.0001 (significant correlation or colocalization); †††p < 0.0001 (significant noncorrelation or noncolocalization compared to random displacement images). Scale bars: (CA1) 5 μm; (others) 10 μm.

Consistently, genomic qPCR showed no increase in the copy number of a region in exon 1 of *Cdx1*, whereas the region proximal to the 5′ end of exon 2 showed twice the copy number of WT controls (Figure 4C). The qPCR results from mRNA demonstrated that the overexpression of *Cdx1* is essentially derived only from exons 2 and 3 of *Cdx1* (Figure 4B), indicating that *Cdx1* overexpression is derived from the BAC transgene. An increase in the gene copy number generally results in upregulated expression, sometimes disproportionately higher in a tandem arrangement (Loehlin and Carroll, 2016), and the "passenger genes" on BAC clones are known to be upregulated in BAC transgenic mice (Farrar et al., 2021; Gong et al., 2010; Ramirez-Fernandez et al., 2020). In addition, considering the fact that the upregulation of *Slc6a7*, *Arsi*, and *Cdx1* unnaturally stands out in terms of fold change and reliability compared to more mild and variable changes in other genes in RNA-seq analysis (Figure S3B and Table S1), it is highly likely that a significant proportion of these upregulated genes is the result of multiplied copy number of genes from the integrated BAC transgene. This issue may be common to Tg(Camk2a-cre/ERT2)2Gsc, the most widely used inducible type of CaMKIIα-Cre line (Figure S1A), as it uses a common BAC clone structure with two copies (Erdmann et al., 2007).

Although the *Syt2* overexpression in CamiCre^{+} brain clearly stands out in the same manner as other BAC transgenes (Figure S3B), *Syt2* copy number was unchanged (Figure 4C). We hypothesized that

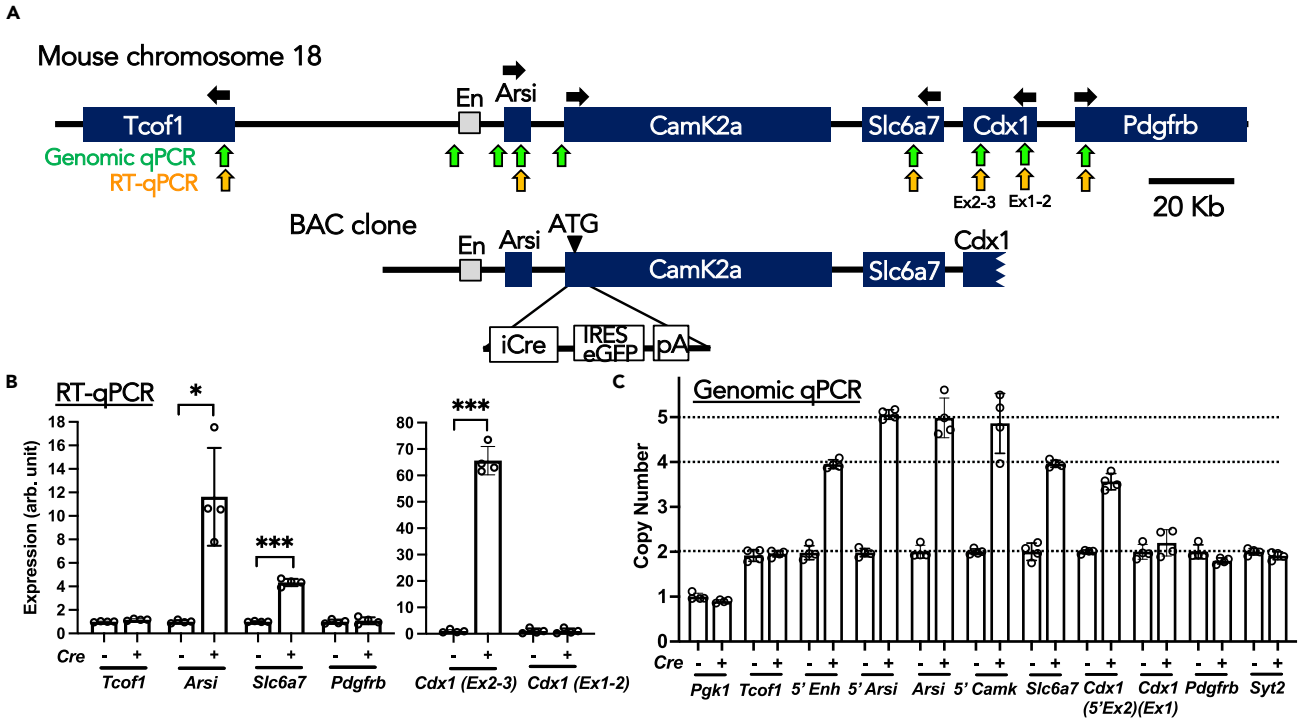

Figure 4. Multiplication of gene copy numbers and upregulation of corresponding genes in CamiCre$^+$ brain

(A) Schematic representation of the genomic structure, BAC clone, and iCre construct. Genes flanking CamK2a are represented by indigo boxes. The gray box represents the enhancer mm879. The structure of the iCre construct inserted in-frame at the ATG site of *CamK2a* is based on Casanova et al. (2001), but the exact size is not represented. Black arrows show the directions of genes. Green and orange arrows represent approximate regions targeted by genomic qPCR and RT-qPCR, respectively.

(B) RT-qPCR analysis (spanning intron) in the hippocampus of CamiCre line. Values were normalized by *Gapdh* expression level and are shown as fold increases against Cre$^-$ controls. Ct values for *Cdx1* (Ex1-2), and *Cdx1* (Ex2-3) in Cre$^-$ were in the range of 32–38, which may be difficult to reliably quantify. Ct values for *Cdx1* (Ex2-3) in Cre$^+$ were approximately 27.

(C) Genomic qPCR analysis of DNA from the male hippocampus of the CamiCre line. *Pgk1* is located on the X chromosome. Mean ± SD is shown. *p < 0.05; ***p < 0.001. N = 4 biological (B) or technical (C) replicates. Statistical tests were performed using two-tailed, unpaired t-tests. See also Figure S3B.

the BAC transgene is inserted in proximity to the *Syt2* locus to disrupt its native suppression machinery, which regulates its precise expression pattern in various neuronal types (Fox and Sanes, 2007; Pang et al., 2006). We investigated this hypothesis by performing Targeted Locus Amplification (TLA) analysis, which is effective in identifying transgene integration site by applying next-generation sequencing on amplified target loci (de Vree et al., 2014). Results of TLA sequencing identified three possible integration sites within a small region (3672 bp) of the *Syt2* locus on chromosome 1 (Figures 5A and 5B). The integration site resides in intron 2 of the longer *Syt2* splice variant, which also corresponds to the 5′ upstream region of the first exon for the shorter variant (Figure 5B). The two variants differ only in the length of the 5′ untranslated region and have the same coding sequences. Variant coverage analysis using RNA-seq data indicated that upregulated mRNA in the CamiCre$^+$ hippocampus is only from the shorter *Syt2* variant (Figure S4). These results strongly suggest that the BAC transgene insertion within the *Syt2* locus dissociated the suppression machinery in the upstream of the longer *Syt2* variant from the shorter *Syt2* variant, which resulted in aberrant overexpression of the shorter *Syt2* variant in CamiCre$^+$ brain.

Lastly, in the T29-1 Cre$^+$ hippocampus, *St6gal2*, a gene encoding beta-galactoside alpha-2,6-sialyltransferase 2, was overexpressed (3.6-fold the level of controls) with very high confidence (Table S2). The physiological role of *St6gal2* is not well studied, but it is implicated in schizophrenia (Ikeda et al., 2010) and autism (Guo et al., 2017). The mechanism of this upregulation is not known, but is likely related to the transgene insertion effect, as low Cre expression in T29-1 is unfavorable for the recombination of pseudo-loxP sites (Carow et al., 2016; Harno et al., 2013), and *St6gal2* upregulation is not observed in CamiCre$^+$ mice.

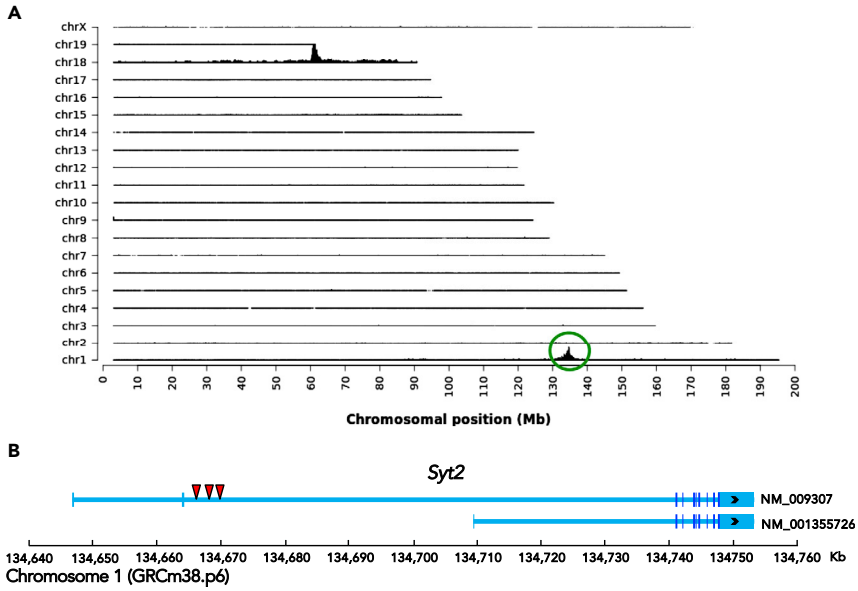

Figure 5. BAC transgene integration sites are within the *Syt2* locus on chromosome one of CamiCre$^+$ mice

(A) Results of TLA sequence coverage across the mouse genome. Chromosomes are indicated on the y axis, and the chromosomal position is shown on the x axis. The identified integration site is encircled in green. The coverage peak on chromosome 18 is owing to the homology of the BAC transgene with the endogenous genome.

(B) Break points for BAC transgene integration sites were identified by TLA sequencing. Coding and noncoding regions in exons are indicated by indigo and light blue boxes, respectively. Red arrowheads indicate the three integration sites at positions 134,666,219, 134,668,306, and 134,669,891 of mouse chromosome 1 (GRC m38). See also Figure S4.

CamiCre$^+$ mice show the upregulation of immediate-early genes and behavioral phenotypes such as hyperactivity and enhanced learning in fear conditioning

We performed Ingenuity Pathway Analysis (IPA) on candidate differentially expressed genes to see whether there is a specific group of genes in signaling pathways that are consistently up- or downregulated. The results suggested the upregulation of the CREB signaling pathway in CamiCre$^+$ hippocampus and we noticed that most of the top-ranking pathways identified included upregulation of immediate-early genes (IEGs) such as *Arc*, *Fos*, *Egr2*, and *Nr4a1* (Table S3). IEGs are rapidly and transiently transcribed genes in response to neuronal stimulation without a requirement for new protein synthesis and are thought to reflect neuronal activity (Yap and Greenberg, 2018). The extent of upregulation of IEGs in CamiCre$^+$ hippocampus was relatively small (20–70% upregulated) in our bulk analysis, but the tendency was clear compared to results from T29-1 Cre$^+$ hippocampus (Figure S3C, Tables S1, and S2). Moreover, the upregulation can be confirmed by qPCR analysis (Figure S3D). These results suggest that neuronal networks in CamiCre$^+$ hippocampus tend to be more activated than in their WT littermates, which is consistent with the idea that the faster release kinetics of overexpressed Syt2 result in more efficient neuronal activity. In addition, *Slc6a7*, which functions as an L-proline transporter, may also be involved, as it is postulated to positively regulate glutamatergic neurotransmission (Schulz et al., 2018). As for the IPA upstream analysis of the T29-1 Cre$^+$ hippocampus, estrogen receptor 1 (ESR1) signaling was suggested to be activated (Table S4).

As *Slc6a7* may also play an important functional role in CamiCre$^+$ mice, we investigated whether SLC6A7 is upregulated at the protein level, together with ARSI (Figure 6A). CDX1 was omitted owing to its truncated nature. SLC6A7 was upregulated 2-fold, whereas no upregulation was detected for ARSI (Figure 6B). We further performed immunostaining of SLC6A7 in CamiCre brains. Consistent with reports showing its presynaptic localization (Crump et al., 1999; Renick et al., 1999), SLC6A7 was stained mainly in the neuropil region, similar to synapsin1/2, a presynaptic marker (Figure 6C). SLC6A7 staining in Cre$^+$ brains showed a mostly similar pattern with relatively higher intensities compared to WT controls. However, CamiCre$^+$ brain showed clear ectopic expression of SLC6A7 in hippocampal mossy fibers, where it was originally absent in WT hippocampus (Renick et al., 1999) (Figure 6C). This aberrant expression pattern likely resulted from a different regulatory mechanism of *Slc6a7* in endogenous locus on chromosome 18 and in integrated

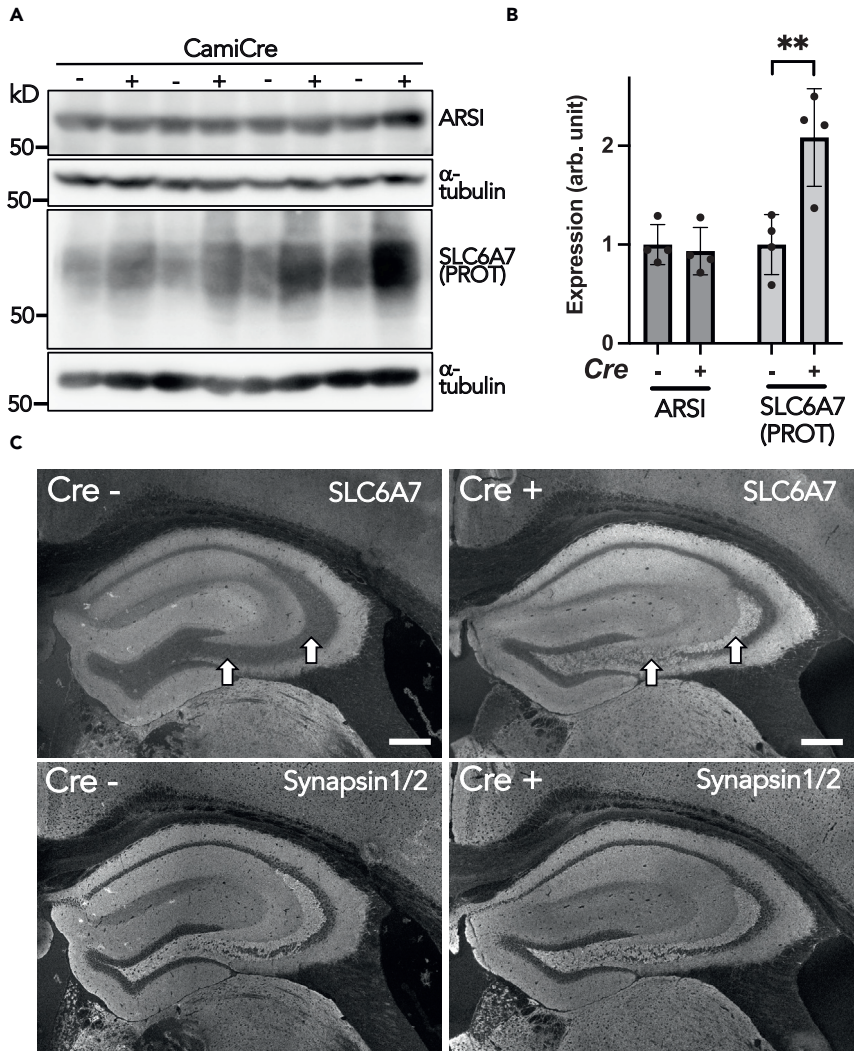

Figure 6. SLC6A7 protein is upregulated and shows ectopic expression in CamiCre$^+$ hippocampus

(A) Western blotting results from hippocampal lysates.

(B) Quantification results of A. Values were normalized against α-tubulin expression level and are shown as fold increases against Cre$^-$ controls. Mean ± SD is shown. **$p < 0.01$. N = 4 (biological replicates). Statistical tests were performed using two-tailed, unpaired t-tests.

(C) Immunofluorescent images of SLC6A7 or Synapsin1/2 staining in the hippocampal region of CamiCre mice. Arrows point to mossy fibers projecting from granule cells in the dentate gyrus. Scale bars: 250 μm.

BAC transgene on chromosome 1. The ectopic and/or enhanced expression of SLC6A7 may also contribute to enhanced hippocampal neural activities.

Finally, and most importantly, with a battery of common behavioral tests, we asked whether CamiCre$^+$ mice show any functional phenotypes. CamiCre$^+$ mice and their littermate controls were examined in the open field, elevated plus maze, y-maze, light-dark transition, cued and contextual fear conditioning, and forced swim tests. CamiCre$^+$ mice traveled significantly farther in the 15-min open field test (Figure 7A). This was owing to enhanced speed and extended duration per movement episode (Figures 7B–7D). CamiCre$^+$ mice did not show a significant difference in the time spent near the center in the open field test, the time spent in the open arms in the elevated plus maze, or the time spent in the light box in a light-dark transition test (Figures S5A–S5C). These results all suggest normal anxiety levels in CamiCre$^+$ mice. They also did not show a significant difference in the forced swim test (Figure S5D), which is used to test despair and depression. However, despite their hyperactivity and normal anxiety levels, CamiCre$^+$ mice showed more freezing

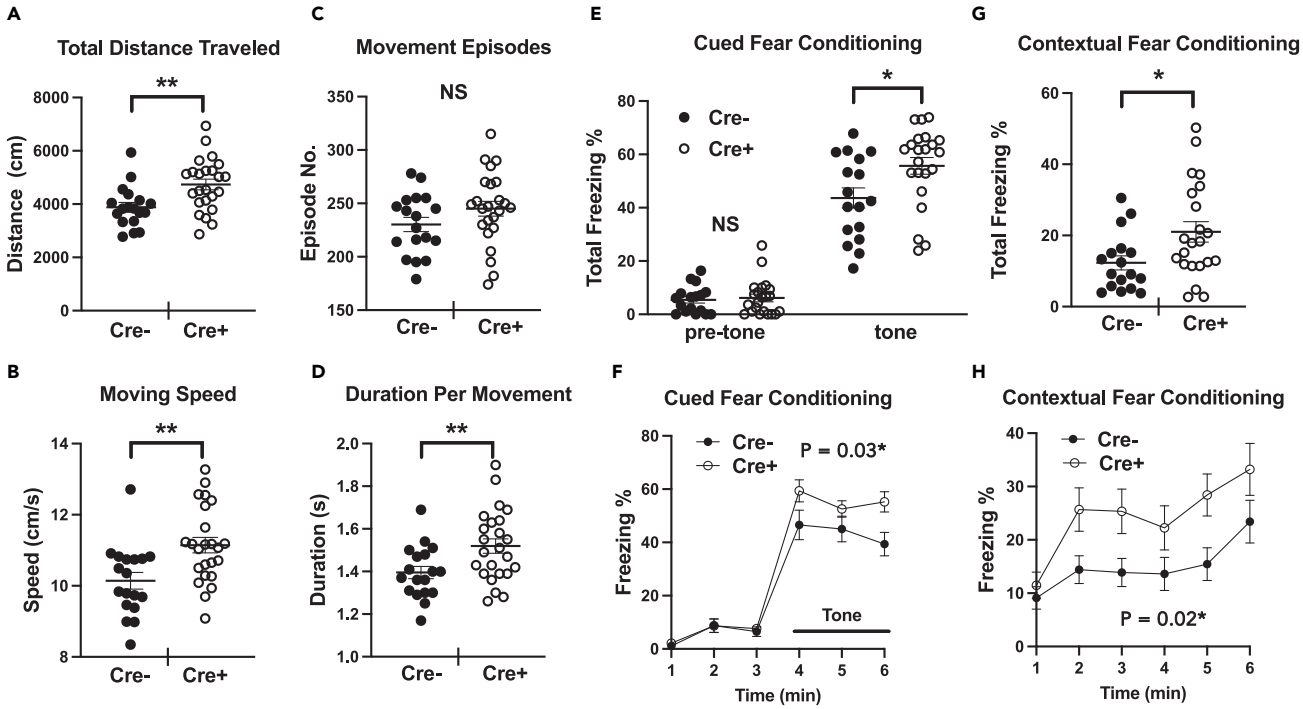

Figure 7. CamiCre$^+$ mice show hyperactivity and enhanced learning in fear conditioning

(A–D) Open field test.

(E–H) Cued and contextual fear conditioning. Mean ± SEM is shown. NS, not significant; *$p < 0.05$; **$p < 0.01$. p values labeled in the line graphs indicate the genotype effect of two-way ANOVA; (F) $F(1, 37) = 5.023$, (H) $F(1, 37) = 6.204$. N = 18 for Cre$^-$, N = 24 for Cre$^+$ for open field test and N = 17 for Cre$^-$, N = 22 for Cre$^+$ for cued and contextual fear conditioning. Statistical tests were performed using two-tailed, unpaired t-tests (A-E), two-tailed Welch's *t* tests (G), or a two-way ANOVA (F, H). Mice that showed significant freezing before the first conditioned stimulus were excluded from the fear conditioning analysis. See also Figure S5.

in both cued and contextual fear conditioning (Figures 7E–7H), which is indicative of better associative learning. On the other hand, they did not show significant differences in short-term spatial working memory in the y-maze test (Figure S4E), but showed increased arm entry numbers, reflecting their hyperactivity (Figure S5F). The hyperactivity and enhanced associative learning phenotypes may also be attributed to overexpression of Syt2 in excitatory presynapses, which should promote faster and more efficient neuronal signaling in CamiCre$^+$ brains. Upregulation of SLC6A7 may also be involved, as *Slc6a7*-deficient mice show reduced locomotor activity and impaired memory extinction (Schulz et al., 2018). *Slc6a7* is also implicated in autism, schizophrenia, and intellectual disability (Schulz et al., 2018).

Potential problems in using CamiCre mice or cre driver lines in general and ways to minimize them

In this report, we demonstrated that Syt2 is ectopically overexpressed in excitatory presynapses of the cerebrum, and SLC6A7 is ectopically overexpressed in hippocampal mossy fibers of CamiCre$^+$ mice. Moreover, transcriptomic analyses indicate that there are many differentially expressed genes in CamiCre$^+$ hippocampi, including IEGs. The biggest drawback is that activities of neural circuits of CamiCre$^+$ mice are likely affected, as suggested by their hyperactivity and better learning in the fear conditioning test. These properties of CamiCre mice clearly pose a problem when utilizing them as Cre drivers, because the purpose is usually to examine the effect of the Cre-driven KO/KI of a gene of interest on neuronal function and its output behavior. Having said that, phenotypes of transcriptomic analyses and behavioral tests shown here could be considered mild compared to many severe phenotypes reported in the literature using CamiCre mice. Therefore, this work does not necessarily invalidate all previous reports using CamiCre mice. Nevertheless, phenotypes shown here are not trivial either, and results obtained using CamiCre mice should be interpreted with caution. In addition, we have also shown that the most widely used T29-1 line also has differential expression in Cre$^+$ mice, which may affect their phenotypes. However, the original articles for this line have described no overt behavioral abnormalities (Tsien et al., 1996a), and no phenotypes

for some of the electrophysiological properties and spatial learning (Tsien et al., 1996b). Whether T29-1 has functional phenotypes under particular conditions require further investigations.

We have read at least two articles that report overexpression of Syt2 as a phenotype reflecting the deletion of a gene of interest using the CaMKIIα-Cre line, that does not clearly state which specific lines they used, but one shows a similar ectopic overexpression pattern in the hippocampus (Park et al., 2019) and the other shows concurrent upregulation of *Slc6a7* and *Arsi* (Wrackmeyer et al., 2019), suggesting the use of the CamiCre line. As these two articles used only *Gene*$^{flox/flox}$ controls, their results should be confirmed with Cre^{+} controls.

One of the simplest ways to minimize problems inherited in a Cre driver line is to include Cre^{+} controls. Various authors have urged the routine use of Cre^{+} controls to circumvent numerous pitfalls in the Cre-loxP system and to correctly interpret data from conditional knockout studies (Becher et al., 2018; Carow et al., 2016; Harno et al., 2013; Lee et al., 2006; Schmidt-Supprian and Rajewsky, 2007). Unfortunately, however, these recommendations are still often neglected. In the case of CamiCre mice, only 15 out of 126 articles clearly mention the use of Cre^{+} controls (Figure S1B) and *Gene*$^{flox/flox}$ or *Gene*$^{flox/+}$; Cre^{-} controls are most frequently used.

Although Cre^{+} controls could clarify whether Cre^{+} itself affects phenotypes of conditional mutant mice to a certain extent, there is a limit. It is possible that phenotypes inherited in Cre driver lines could enhance or cancel true phenotypes of mutations of interest. Moreover, synergistic phenotypes of Cre mice with mutated genes of interest may be unpredictable and different from original phenotypes. These results may not always be clarified by Cre^{+} controls. One way to circumvent this issue is to find Cre driver lines that are established to have minimal phenotypes in systems of interest. However, using Cre^{+} controls is still important, as phenotypes could change with age, genetic background, housing environment, and experimenter handling of the mice. In cases in which researchers need to use a particular Cre driver line with a potentially problematic phenotype for a specific expression region and/or Cre recombination efficiency, another way to circumvent the issue is to show similar results in different systems, such as different Cre line(s) with the same or different promotors, conventional KO lines (if applicable), AAV-Cre-mediated KO mice, or RNAi/CRISPR-Cas9 mediated KDs/KOs in cell cultures (if applicable). These additional datasets could confirm that results are independent of a problematic Cre driver line.

The BAC transgene strategy has proven effective in mimicking the true expression pattern of target genes, but the existence of passenger genes on BAC clones may occasionally be difficult to avoid (Farrar et al., 2021; Gong et al., 2010; Ramirez-Fernandez et al., 2020) and could produce unexpected phenotypes, as shown for the CamiCre line. One way to avoid this from the creator side may be to induce mutations to disrupt the expression of passenger genes in BAC DNA, before its integration into the mouse genome. For example, mutations in initiation codons, introduction of stop codons, and/or induced frame shifts may stop the production of functional proteins.

To our knowledge, while Cre driver lines are well characterized for Cre expression patterns, many are not well characterized for phenotypes unless they are obvious, and most genomic locations of transgene insertion are not known. This work shows the effectiveness of utilizing comprehensive transcriptome analysis on a Cre driver line for screening extreme changes in gene expression, which could result from transgene insertions, unintended recombination at pseudo-loxP sites, or even Cre toxicity (Becher et al., 2018; Carow et al., 2016; Harno et al., 2013; Lee et al., 2006; Schmidt-Supprian and Rajewsky, 2007). General assessment of the status of a tissue or a cell type of interest by pathway analyses is also informative. Perhaps creating a database of DE analyses for Cre driver lines would benefit researchers in choosing the right driver line for their research and the appropriate interpretation of their results. We hope this work will raise awareness of potential caveats to using the Cre-loxP system in general and will encourage researchers to be cautious in designing control experiments to maximize the utility of the system and the validity of their results.

Limitations of the study

In this work, we focused on the ectopic expression of Syt2 in regions from forebrain where it is clearly overexpressed, as shown by Western blotting. However, it is possible that Syt2 is also ectopically expressed in portions of some caudal brain regions that are difficult to detect in bulk analyses such as Western blotting.

This work did not determine whether Syt2 is also overexpressed in the originally expressed regions such as in inhibitory presynapses. The exact integration events of BAC transgenes could not be determined in our TLA analyses owing to high complexity. Although it is very likely that overexpression of *Slc6a7* and *Arsi* is derived from integrated BAC transgenes similar tod *Cdx1*, we could not provide direct experimental evidence, as the genes on BAC are the same as endogenous genes and there is no way to distinguish the source. Therefore, it is possible that some of this overexpression is from endogenous genes, although we have no data to suggest any factors that could activate these two endogenous genes or reasons to believe that two genes on the BAC transgene are silenced. This work did not address the ectopic expression of SLC6A7 at subcellular resolution.

STAR★METHODS

Detailed methods are provided in the online version of this paper and include the following:

- KEY RESOURCES TABLE
- RESOURCE AVAILABILITY
  - Lead contact
  - Materials availability
  - Data and code availability
- EXPERIMENTAL MODEL AND SUBJECT DETAILS
  - Mice
- METHOD DETAILS
  - Literature survey
  - RT-qPCR
  - Western blotting
  - AAV injection
  - Immunohistochemistry
  - Colocalization analysis
  - RNA-seq and DE analysis
  - Genomic qPCR
  - Targeted Locus Amplification (TLA) analysis
  - Behavioral analysis
  - Open field test
  - Elevated plus maze
  - Y-maze
  - Light-dark transition test
  - Contextual and cued fear conditioning
  - Forced swim test
- QUANTIFICATION AND STATISTICAL ANALYSIS

SUPPLEMENTAL INFORMATION

Supplemental information can be found online at https://doi.org/10.1016/j.isci.2022.104692.

ACKNOWLEDGMENTS

We thank Drs. Shigeyoshi Itohara and Takuji Iwasato (RIKEN Brain Science Institute) for providing $Emx1^{tm1(cre)Ito}$ mice. We thank Dr. Bernd Kuhn (Optical Neuroimaging Unit, OIST) for technical support on AAV injections. pENN.AAV.hSyn.Cre.WPRE.hGH and pAAV.hSyn.eGFP.WPRE.bGH were gifts from James M. Wilson. We are grateful for the help and support provided by the Animal Resource Section and the Sequencing Section of the Research Support Division at Okinawa Institute of Science and Technology Graduate University (OIST). The graphical abstract was created using Biorender. This work was supported by JSPS KAKENHI Grant Number JP19K07394.

AUTHOR CONTRIBUTIONS

Conceptualization: KM, Methodology: KM, HMAM, MMMY, Investigation: KM, HMAM, MMMY, Visualization: KM, Funding acquisition: KM, TY, Project administration: KM, TY, Supervision: KM, YY, TY, Writing – original draft: KM, Writing – review & editing: KM, HMAM, MMMY, YY, TY.

DECLARATION OF INTERESTS

The authors declare no competing interests.

Received: August 30, 2021
Revised: April 29, 2022
Accepted: June 27, 2022
Published: August 19, 2022

REFERENCES

Amend, S.R., Valkenburg, K.C., and Pienta, K.J. (2016). Murine hind limb long bone dissection and bone marrow isolation. J Vis Exp. https://doi.org/10.3791/53936.

Augustinaite, S., and Kuhn, B. (2020). Complementary Ca(2+) activity of sensory activated and suppressed layer 6 corticothalamic neurons reflects behavioral state. Curr. Biol. *30*, 3945–3960.e5. https://doi.org/10.1016/j.cub.2020.07.069.

Becher, B., Waisman, A., and Lu, L.F. (2018). Conditional gene-targeting in mice: problems and solutions. Immunity *48*, 835–836. https://doi.org/10.1016/j.immuni.2018.05.002.

Branda, C.S., and Dymecki, S.M. (2004). Talking about a revolution: the impact of site-specific recombinases on genetic analyses in mice. Dev. Cell. *6*, 7–28. https://doi.org/10.1016/s1534-5807(03)00399-x.

Bult, C.J., Blake, J.A., Smith, C.L., Kadin, J.A., and Richardson, J.E. (2019). Mouse genome database (MGD) 2019. Nucleic. Acids. Res. *47*, D801–D806. https://doi.org/10.1093/nar/gky1056.

Carow, B., Gao, Y., Coquet, J., Reilly, M., and Rottenberg, M.E. (2016). Lck-driven cre expression alters T cell development in the thymus and the frequencies and functions of peripheral T cell subsets. J. Immunol. *197*, 2261–2268. https://doi.org/10.4049/jimmunol.1600827.

Casanova, E., Fehsenfeld, S., Mantamadiotis, T., Lemberger, T., Greiner, E., Stewart, A.F., and Schütz, G. (2001). A CamKIIα iCre BAC allows brain-specific gene inactivation. Genesis *31*, 37–42. https://doi.org/10.1002/gene.1078.

Cedernaes, J., Huang, W., Ramsey, K.M., Waldeck, N., Cheng, L., Marcheva, B., Omura, C., Kobayashi, Y., Peek, C.B., Levine, D.C., et al. (2019). Transcriptional basis for rhythmic control of hunger and metabolism within the AgRP neuron. Cell Metabol. *29*, 1078–1091.e5. https://doi.org/10.1016/j.cmet.2019.01.023.

Chen, C., Arai, I., Satterfield, R., Young, S.M., Jr., and Jonas, P. (2017). Synaptotagmin 2 is the fast Ca(2+) sensor at a central inhibitory synapse. Cell Rep. *18*, 723–736. https://doi.org/10.1016/j.celrep.2016.12.067.

Crump, F., Fremeau, R.T., and Craig, A.M. (1999). Localization of the brain-specific high-affinity l-proline transporter in cultured hippocampal neurons: molecular heterogeneity of synaptic terminals. Mol. Cell. Neurosci. *13*, 25–39. https://doi.org/10.1006/mcne.1998.0727.

Daigle, T.L., Madisen, L., Hage, T.A., Valley, M.T., Knoblich, U., Larsen, R.S., Takeno, M.M., Huang, L., Gu, H., Larsen, R., et al. (2018). A suite of transgenic driver and reporter mouse lines with enhanced brain-cell-type targeting and functionality. Cell *174*, 465–480.e22. https://doi.org/10.1016/j.cell.2018.06.035.

de Vree, P.J.P., de Wit, E., Yilmaz, M., van de Heijning, M., Klous, P., Verstegen, M.J.A.M., Wan, Y., Teunissen, H., Krijger, P.H.L., Geeven, G., et al. (2014). Targeted sequencing by proximity ligation for comprehensive variant detection and local haplotyping. Nat. Biotechnol. *32*, 1019–1025. https://doi.org/10.1038/nbt.2959.

Dobin, A., Davis, C.A., Schlesinger, F., Drenkow, J., Zaleski, C., Jha, S., Batut, P., Chaisson, M., and Gingeras, T.R. (2013). STAR: ultrafast universal RNA-seq aligner. Bioinformatics *29*, 15–21. https://doi.org/10.1093/bioinformatics/bts635.

Erdmann, G., Schütz, G., and Berger, S. (2007). Inducible gene inactivation in neurons of the adult mouse forebrain. BMC. Neurosci. *8*, 63. https://doi.org/10.1186/1471-2202-8-63.

Ewels, P.A., Peltzer, A., Fillinger, S., Patel, H., Alneberg, J., Wilm, A., Garcia, M.U., Di Tommaso, P., and Nahnsen, S. (2020). The nf-core framework for community-curated bioinformatics pipelines. Nat. Biotechnol. *38*, 276–278. https://doi.org/10.1038/s41587-020-0439-x.

Farrar, J.S., Lownik, J.C., Way, G.W., Rodriguez, M.C., Celi, F.S., and Martin, R.K. (2021). Identification of the transgene insertion site for an adipocyte-specific adiponectin-cre model and characterization of the functional consequences. Adipocyte *10*, 91–100. https://doi.org/10.1080/21623945.2021.1880083.

Fox, M.A., and Sanes, J.R. (2007). Synaptotagmin I and II are present in distinct subsets of central synapses. J. Comp. Neurol. *503*, 280–296. https://doi.org/10.1002/cne.21381.

Gerfen, C., Paletzki, R., and Heintz, N. (2013). GENSAT BAC cre-recombinase driver lines to study the functional organization of cerebral cortical and basal ganglia circuits. Neuron *80*, 1368–1383. https://doi.org/10.1016/j.neuron.2013.10.016.

Godinho-Silva, C., Domingues, R.G., Rendas, M., Raposo, B., Ribeiro, H., da Silva, J.A., Vieira, A., Costa, R.M., Barbosa-Morais, N.L., Carvalho, T., and Veiga-Fernandes, H. (2019). Light-entrained and brain-tuned circadian circuits regulate ILC3s and gut homeostasis. Nature *574*, 254–258. https://doi.org/10.1038/s41586-019-1579-3.

Gong, S., Doughty, M., Harbaugh, C.R., Cummins, A., Hatten, M.E., Heintz, N., and Gerfen, C.R. (2007). Targeting Cre recombinase to specific neuron populations with bacterial artificial chromosome constructs. J. Neurosci. *27*, 9817–9823. https://doi.org/10.1523/jneurosci.2707-07.2007.

Gong, S., Kus, L., and Heintz, N. (2010). Rapid bacterial artificial chromosome modification for large-scale mouse transgenesis. Nat. Protoc. *5*, 1678–1696. https://doi.org/10.1038/nprot.2010.131.

Guo, H., Peng, Y., Hu, Z., Li, Y., Xun, G., Ou, J., Sun, L., Xiong, Z., Liu, Y., Wang, T., et al. (2017). Genome-wide copy number variation analysis in a Chinese autism spectrum disorder cohort. Sci. Rep. *7*, 44155. https://doi.org/10.1038/srep44155.

Harno, E., Cottrell, E., and White, A. (2013). Metabolic pitfalls of CNS Cre-based technology. Cell Metabol. *18*, 21–28. https://doi.org/10.1016/j.cmet.2013.05.019.

Heintz, N. (2001). BAC to the future: the use of bac transgenic mice for neuroscience research. Nat. Rev. Neurosci. *2*, 861–870. https://doi.org/10.1038/35104049.

Ikeda, M., Tomita, Y., Mouri, A., Koga, M., Okochi, T., Yoshimura, R., Yamanouchi, Y., Kinoshita, Y., Hashimoto, R., Williams, H.J., et al. (2010). Identification of novel candidate genes for treatment response to risperidone and susceptibility for schizophrenia: integrated analysis among pharmacogenomics, mouse expression, and genetic case-control association approaches. Biol. Psychiatry. *67*, 263–269. https://doi.org/10.1016/j.biopsych.2009.08.030.

Iwasato, T., Datwani, A., Wolf, A.M., Nishiyama, H., Taguchi, Y., Tonegawa, S., Knöpfel, T., Erzurumlu, R.S., and Itohara, S. (2000). Cortex-restricted disruption of NMDAR1 impairs neuronal patterns in the barrel cortex. Nature *406*, 726–731. https://doi.org/10.1038/35021059.

Lee, J.Y., Ristow, M., Lin, X., White, M.F., Magnuson, M.A., and Hennighausen, L. (2006). RIP-Cre revisited, evidence for impairments of pancreatic beta-cell function. J. Biol. Chem. *281*, 2649–2653. https://doi.org/10.1074/jbc.m512373200.

Liao, Y., Smyth, G.K., and Shi, W. (2014). featureCounts: an efficient general purpose program for assigning sequence reads to genomic features. Bioinformatics *30*, 923–930. https://doi.org/10.1093/bioinformatics/btt656.

Loehlin, D.W., and Carroll, S.B. (2016). Expression of tandem gene duplicates is often greater than twofold. Proc. Natl. Acad. Sci. USA *113*, 5988–5992. https://doi.org/10.1073/pnas.1605886113.

Matsuura, K., Kobayashi, S., Konno, K., Yamasaki, M., Horiuchi, T., Senda, T., Hayashi, T., Satoh, K., Arima-Yoshida, F., Iwasaki, K., et al. (2022).

SIPA1L1/SPAR1 interacts with the neurabin family of proteins and is involved in GPCR signaling. J. Neurosci. *42*, 2448–2473. https://doi.org/10.1523/jneurosci.0569-21.2022.

Pang, Z.P., Melicoff, E., Padgett, D., Liu, Y., Teich, A.F., Dickey, B.F., Lin, W., Adachi, R., and Sudhof, T.C. (2006). Synaptotagmin-2 is essential for survival and contributes to Ca2+ triggering of neurotransmitter release in central and neuromuscular synapses. J. Neurosci. *26*, 13493–13504. https://doi.org/10.1523/jneurosci.3519-06.2006.

Park, J., Park, S.J., and Kim, S. (2019). Inositol polyphosphate multikinase deficiency leads to aberrant induction of synaptotagmin-2 in the forebrain. Mol. Brain *12*, 58. https://doi.org/10.1186/s13041-019-0480-1.

Ramírez, O., García, A., Rojas, R., Couve, A., and Härtel, S. (2010). Confined displacement algorithm determines true and random colocalization in fluorescence microscopy. J. Microsc. *239*, 173–183. https://doi.org/10.1111/j.1365-2818.2010.03369.x.

Ramírez-Fernández, A., Urbina-Treviño, L., Conte, G., Alves, M., Rissiek, B., Durner, A., Scalbert, N., Zhang, J., Magnus, T., Koch-Nolte, F., et al. (2020). Deviant reporter expression and P2X4 passenger gene overexpression in the soluble EGFP BAC transgenic P2X7 reporter mouse model. Sci. Rep. *10*, 19876. https://doi.org/10.1038/s41598-020-76428-0.

Renick, S.E., Kleven, D.T., Chan, J., Stenius, K., Milner, T.A., Pickel, V.M., and Fremeau, R.T., Jr. (1999). The mammalian brain high-affinity L-proline transporter is enriched preferentially in synaptic vesicles in a subpopulation of excitatory nerve terminals in rat forebrain. J. Neurosci. *19*, 21–33. https://doi.org/10.1523/jneurosci.19-01-00021.1999.

Robinson, M.D., McCarthy, D.J., and Smyth, G.K. (2010). edgeR: a Bioconductor package for differential expression analysis of digital gene expression data. Bioinformatics *26*, 139–140. https://doi.org/10.1093/bioinformatics/btp616.

Schindelin, J., Arganda-Carreras, I., Frise, E., Kaynig, V., Longair, M., Pietzsch, T., Preibisch, S., Rueden, C., Saalfeld, S., Schmid, B., et al. (2012). Fiji: an open-source platform for biological-image analysis. Nat. Methods *9*, 676–682. https://doi.org/10.1038/nmeth.2019.

Schmidt-Supprian, M., and Rajewsky, K. (2007). Vagaries of conditional gene targeting. Nat. Immunol. *8*, 665–668. https://doi.org/10.1038/ni0707-665.

Schulz, D., Morschel, J., Schuster, S., Eulenburg, V., and Gomeza, J. (2018). Inactivation of the mouse L-proline transporter PROT alters glutamatergic synapse biochemistry and perturbs behaviors required to respond to environmental changes. Front. Mol. Neurosci. *11*, 279. https://doi.org/10.3389/fnmol.2018.00279.

Shimshek, D.R., Kim, J., Hübner, M., Spergel, D.J., Buchholz, F., Casanova, E., Stewart, A.F., Seeburg, P.H., and Sprengel, R. (2002). Codon-improved Cre recombinase (iCre) expression in the mouse. Genesis *32*, 19–26. https://doi.org/10.1002/gene.10023.

Tsien, J.Z., Chen, D.F., Gerber, D., Tom, C., Mercer, E.H., Anderson, D.J., Mayford, M., Kandel, E.R., and Tonegawa, S. (1996a). Subregion- and cell type-restricted gene knockout in mouse brain. Cell *87*, 1317–1326. https://doi.org/10.1016/s0092-8674(00)81826-7.

Tsien, J.Z., Huerta, P.T., and Tonegawa, S. (1996b). The essential role of hippocampal CA1 NMDA receptor-dependent synaptic plasticity in spatial memory. Cell *87*, 1327–1338. https://doi.org/10.1016/s0092-8674(00)81827-9.

Wrackmeyer, U., Kaldrack, J., Jüttner, R., Pannasch, U., Gimber, N., Freiberg, F., Purfürst, B., Kainmueller, D., Schmitz, D., Haucke, V., et al. (2019). The cell adhesion protein CAR is a negative regulator of synaptic transmission. Sci. Rep. *9*, 6768. https://doi.org/10.1038/s41598-019-43150-5.

Xu, J., Mashimo, T., and Südhof, T.C. (2007). Synaptotagmin-1, -2, and -9: Ca(2+) sensors for fast release that specify distinct presynaptic properties in subsets of neurons. Neuron *54*, 567–581. https://doi.org/10.1016/j.neuron.2007.05.004.

Yap, E.L., and Greenberg, M.E. (2018). Activity-regulated transcription: bridging the gap between neural activity and behavior. Neuron *100*, 330–348. https://doi.org/10.1016/j.neuron.2018.10.013.

Zhou, M., Melin, M.D., Xu, W., and Südhof, T.C. (2020). Dysfunction of parvalbumin neurons in the cerebellar nuclei produces an action tremor. J. Clin. Invest. *130*, 5142–5156. https://doi.org/10.1172/jci135802.

STAR★METHODS

KEY RESOURCES TABLE

REAGENT or RESOURCE	SOURCE	IDENTIFIER
Antibodies		
Rabbit polyclonal antibody anti-Syt1	Synaptic Systems	Cat#105103; RRID:AB_11042457
Mouse monoclonal antibody anti-Syt2 (clone ZNP-1)	Abcam	Cat#ab154035; RRID: AB_2916272
Rabbit polyclonal antibody anti-Cre	Cell Signaling	Cat#15036S; RRID:AB_2798694
Mouse monoclonal antibody anti-a-tubulin (clone DM1A)	Sigma-Aldrich	Cat#T6199; RRID:AB_477583
Rabbit polyclonal antibody anti-ARSI	Thermo Fisher Scientific	Cat#PA5-49984; RRID:AB_2635437
Rabbit polyclonal antibody anti- SLC6A7	almone labs	Cat#AGT-013; RRID:AB_2756640
Rabbit polyclonal antibody anti-VGluT1	Millipore	Cat#ABN1647; RRID:AB_2814811
Guinea pig polyclonal antibody anti-synapsin1/2	Synaptic Systems	Cat#106004; RRID:AB_1106784
Bacterial and virus strains		
AAV1.hSyn.Cre.WPRE.hGH	Addgene	Addgene AAV1; 105553-AAV1
AAV1.hSyn.eGFP.WPRE.bGH	Addgene	Addgene AAV1; 105539-AAV1
Chemicals, peptides, and recombinant proteins		
Tissue-Tek OCT compound	Sakura Finetek	Cat#4583
Critical commercial assays		
Isogen II reagent	Nippon Gene	Cat#311-07361
PrimeScript II 1st strand cDNA Synthesis Kit	TAKARA	Cat#6210A
TB Green Premix Ex Taq II (Tli RNaseH Plus)	TAKARA	Cat#RR820B
Can Get Signal Immunoreaction Enhancer Solution	TOYOBO	Cat#NKB-101
Immobilon	Merck	Cat#WBKLS0500
Western Lightning Plus-ECL	Perkin Elmer	Cat#NEL105001EA
Restore Plus Western Blot Stripping Buffer	Thermo Scientific	Cat#46430
M.O.M. (Mouse on Mouse) Immunodetection Kit	Vector Laboratories	Cat#BMK-2202
Vectashield mounting medium	Vector Laboratories	Cat#H-1000
NEBNext Poly(A) mRNA Magnetic Isolation Module	New England BioLabs	Cat#E7490L
NEBNext Ultra II Directional RNA Library Prep Kit for Illumina	New England BioLabs	Cat#E7760L
NucleoSpin Tissue	MACHEREY-NAGEL	Cat#740952.10
Deposited data		
RNA-seq data	This paper	GEO: GSE179804
TLA sequencing data	This paper	SRA: SAMN27916987
TLA sequencing data	This paper	SRA: SAMN27916988
TLA sequencing data	This paper	SRA: SAMN27916989
TLA sequencing data	This paper	SRA: SAMN27916990
Experimental models: Organisms/strains		
B6.FVB-Tg(Camk2a-cre)2Gsc/Cnrm	EMMA	EM:01153; RRID:MGI:4457404
B6.Cg-Tg(Camk2a-cre)T29-1Stl/J	The Jackson Laboratory	RRID:IMSR_JAX:005359
B6.129P2-Emx1$^{tm1(cre)Ito}$/ItoRbrc	RIKEN BRC	RRID:IMSR_RBRC00808
Oligonucleotides		
See Table S5 for primer sequences.		

(*Continued on next page*)

Continued

REAGENT or RESOURCE	SOURCE	IDENTIFIER
Software and algorithms		
Fiji/ImageJ with GDSC ImageJ plug-in	Schindelin et al. (2012); Ramirez et al. (2010)	https://fiji.sc; http://www.sussex.ac.uk/gdsc/intranet/microscopy/UserSupport/AnalysisProtocol/imagej/gdsc_plugins
nf-core/rnaseq pipeline (version 2.0)	Ewels et al. (2020); Liao et al. (2014); Dobin et al. (2013)	https://nf-co.re/rnaseq/2.0
OmicsBox software (version 1.4.11)	BioBam; Robinson et al. (2010)	https://www.biobam.com/omicsbox-update-1-4/?cn-reloaded=1
Strand NGS (version 4.0)	Strand Life Sciences	https://www.strand-ngs.com
Behavioral analyses software series	O'hara & Co.	https://ohara-time.co.jp/category/products/
GraphPad Prism 9	GraphPad Software	https://www.graphpad.com/scientific-software/prism/

RESOURCE AVAILABILITY

Lead contact

Further information and requests for resources and reagents should be directed to the lead contact, Ken Matsuura (ken.matsuura@oist.jp).

Materials availability

This study did not generate new, unique reagents.

Data and code availability

- RNA-seq data and TLA sequencing data have been deposited at GEO and SRA, respectively. They are publicly available as of the date of publication. Accession numbers are listed in the key resources table.
- This paper does not report original code.
- Any additional information required to reanalyze the data reported in this paper is available from the lead contact upon request.

EXPERIMENTAL MODEL AND SUBJECT DETAILS

Mice

The CamiCre line (B6.FVB-Tg(Camk2a-cre)2Gsc/Cnrm) was obtained from EMMA (EM:01153) and backcrossed seven times onto a C57BL/6J genetic background. The T29-1 line (B6.Cg-Tg(Camk2a-cre)T29-1Stl/J) was obtained from The Jackson Laboratory (JAX: 005359). The Emx1Cre line (B6.129P2-Emx1$^{tm1(cre)Ito}$/ItoRbrc) was provided by Drs. Shigeyoshi Itohara and Takuji Iwasato (RBRC00808). The iCre or Cre transgene was kept heterozygous in all lines. Genotyping was performed by genomic PCR. An iCre or Cre primer pair was used in conjunction with an IL2 control pair at a ratio of 3:1 concentration. Primer sequences are listed in Table S5. Mice were kept under a 12-h light/12-h dark cycle in a temperature- and humidity-controlled specific pathogen-free vivarium, and they had *ad libitum* access to food and water. 4-5 mice of the same sex were group-housed in a cage. 7- to 9-week-old healthy male mice weighing 20–25 g were used for all experiments unless noted otherwise. iCre/+ or Cre/+ heterozygous mice and littermate control +/+ mice were used. All animal experiments were conducted according to guidelines for care and use of animals, approved by the Animal Experiment Committee of Okinawa Institute of Science and Technology Graduate University (Approval no. 2016-159 and 2020-283).

METHOD DETAILS

Literature survey

Information was from the Mouse Genome Informatics (MGI) database (Bult et al., 2019). We successfully had access to all links to full text from: http://www.informatics.jax.org/reference/allele/MGI:2181426?

typeFilter=Literature. Each paper was surveyed for the description of control mice and those clearly stating the use of Cre^+ controls were counted.

RT-qPCR

For qPCR, total RNA was extracted from mouse hippocampi using Isogen II reagent (Nippon Gene). Reverse transcription was performed using PrimeScript II 1st strand cDNA Synthesis Kit (TAKARA) following the manufacturer's protocol. Real-time PCR was performed using TB Green Premix Ex Taq II (Tli RNaseH Plus) (TAKARA) and ViiA7 Real-Time PCR system, Software v1.2 (Applied Biosystems) according to the manufacturer's protocol. For detecting introns in premRNA of Syt2, RT (-) controls were used and confirmed for no detection or detection at higher Ct values with distinct melting curves compared to RT (+) samples. Primer sequences are listed in Table S5.

Western blotting

Mouse brain regions of interest were quickly dissected on filter paper soaked with ice-cold PBS, snap frozen in liquid nitrogen and stored at −80 °C. Brain regions were homogenized in ice-cold lysis buffer (0.3% SDS, 1.67% Triton X-100, 50 mM Tris-HCl pH7.4, 150 mM NaCl, 1 mM EDTA, 1 mM EGTA, 1mM PMSF, 1mM Na_3VO_4, 25mM NaF, PI cocktail [5 μg/mL aprotinin, chymostatin, leupeptin and pepstatin A], 10% glycerol) using a pellet mixer, rotated 60 min at 4°C, and centrifuged for 30 min at 20,400 x g, 4°C. Supernatants were collected and adjusted for protein concentration, mixed with 6x SDS sample buffer, and then heated at 56°C for 10 min. Samples were subjected to 8% SDS-PAGE. Western blotting was performed by standard methods. Briefly, proteins were transferred to PVDF membranes (Immobilon, Millipore) and blocked in TBS containing 5% skim milk and 0.1% Tween-20. For antibody dilution, Can Get Signal Immunoreaction Enhancer Solution (TOYOBO) or blocking solution (for α-tubulin and Cre) was used. A chemiluminescent signal was detected using Immobilon (Millipore) or, for α-tubulin, Western Lightning Plus-ECL (Perkin Elmer) on ImageQuant LAS4000 (FujiFilm) following the manufacturer's protocol. Antibodies used were rabbit polyclonal antibody (RpAb) to Syt1 (1:1000) from Synaptic Systems (105103), mouse monoclonal antibody (MmAb) to Syt2 (1:1000) from Abnova (clone ZPN-1), RpAb to Cre (1:1000) from Cell Signaling (15036S), MmAb to α-tubulin (1:1000) from Sigma-Aldrich (clone DM1A), RpAb to ARSI (1:1000) from Thermo Fisher Scientific (PA5-49984), and RpAb to SLC6A7 (1:500) from almone labs (AGT-013). For reprobing, Restore Plus Western Blot Stripping Buffer (Thermo Scientific) was used. Fiji/ImageJ (NIH) (Schindelin et al., 2012) was used for quantification.

AAV injection

Mice were injected with Cre-expressing adeno-associated virus AAV1.hSyn.Cre.WPRE.hGH (105553-AAV1, Addgene; $\geq 1 \times 10^{13}$ vg/ml) and GFP-expressing AAV1.hSyn.eGFP.WPRE.bGH (105539-AAV1, Addgene; $\geq 2.1 \times 10^{13}$ vg/ml). Stereotaxic surgical procedures were performed as described (Augustinaite and Kuhn, 2020). Viral solutions of around 250 nL were slowly injected using sharp tip beveled quartz pipettes into the CA2 regions of the hippocampi, according to the following coordinates (1.6 mm posterior, 1.6 mm lateral and 1.6 mm ventral to bregma). Additionally, AAV-Cre serial dilutions were done using sterile 0.9% saline solution. The titers for serial dilution started with $\geq 2.5 \times 10^{12}$ vg/ml and diluted by two-fold for each dilution.

Immunohistochemistry

Mice were deeply anesthetized with isoflurane and were intracardially perfused with ice-cold sodium phosphate buffer (pH 7.3, NPB), followed by ice-cold 4% paraformaldehyde (PFA) /NPB. The whole brain was removed, separated bilaterally at the medial line and fixed in ice-cold 4% PFA/NPB for 2 h. The brain was further infiltrated sequentially with 10, 15, and 25% sucrose/NPB for more than 4 h at each concentration and then frozen in a Tissue-Tek OCT compound (Sakura Finetek). 10-μm cryosections were attached to an MAS-coated slide glass (S9441 Matsunami) and air dried for 2 h. For permeabilization, sections were incubated in 0.3% Triton X-100/Tris-buffered saline (pH7.5, TBS) for 10 min at room temperature. Sections were blocked with TBS containing a 0.5% blocking reagent (Roche), 2% fetal bovine serum, Mouse Ig Blocking Reagent (Vector Laboratories), and 0.1% Tween-20 for 1 h. Then they were incubated overnight at 4 °C with primary antibodies diluted in a dilution buffer (0.5% blocking reagent (Roche), 2% fetal bovine serum, M.O.M. Protein Concentrate (Vector Laboratories), 0.1% Tween-20, TBS). Following washes in TBS containing 0.1% Tween-20 (TBST), sections were incubated for 1 h at RT with secondary antibodies diluted in dilution buffer. Sections were subsequently stained with DAPI, washed, and coverslipped with Vectashield

mounting medium (Vector Laboratories). Sections from CamiCre$^+$ and control mice were processed simultaneously on the same slide glass. Antibodies used were RpAb to VGluT1 (1:100) from Millipore (ABN1647), MmAb to Syt2 (1:100) from Abcam (clone ZPN-1), RpAb to Cre (1:100) from Cell Signaling (15036S), guinea pig pAb to synapsin1/2 (1:200) from Synaptic Systems (106004), RpAb to SLC6A7 (1:50) from almone labs (AGT-013), Alexa Fluor 488 Goat Anti-mouse IgG (1:300), Alexa Fluor 568 Goat Anti-rabbit IgG (1:300), and Alexa Fluor 647 Donkey Anti-guinea pig IgG (1:300) from Invitrogen. Digital images were obtained using a Leica TCS SP8 LIGHTNING confocal microscope equipped with a motorized stage and LAS X software. Briefly, for low-magnification images, brain regions were scanned using an HC PL APO CS2 10x/0.40 DRY objective and images were stitched automatically using LAS X software. For high-resolution imaging, an HC PL APO CS2 63x/1.40 OIL objective was used in LIGHTNING mode with 120-nm resolution. Images with 3064 x 3064 pixels (47 x 47 nm^2/pixel) were acquired. Original images adjusted only for brightness and contrast with Fiji/ImageJ (NIH) (Schindelin et al., 2012) are shown in the figures.

Colocalization analysis

Colocalization analysis was performed as described previously (Matsuura et al., 2022), using the GDSC ImageJ plug-in (http://www.sussex.ac.uk/gdsc/intranet/microscopy/UserSupport/AnalysisProtocol/imagej/colocalisation). Briefly, high-resolution images stained for Syt2 and VgluT1 in the indicated regions were acquired as described above. Three serial Z-stack images (1-μm step size) of 3064 x 3064 pixels (144.7 x 144.7 μm^2)/image were processed to define foreground and background with the Otsu method using Stack Threshold Plugin. Processed images and original images were used to calculate the statistical significance of Manders coefficient and Pearson correlation coefficient, respectively, with the Confined Displacement Algorithm Plugin. The significance of correlation or colocalization was calculated by comparing original images to random displacement images. The random displacement was defined using radial displacement chart of Pearson correlation coefficient for each sample according to the user manual. A P value of <0.0001 was adopted for statistical significance.

RNA-seq and DE analysis

Total RNA was purified from mouse hippocampi using Isogen II reagent (Nippon Gene). Subsequently, 500 ng of total RNA samples were enriched for mRNA using NEBNext Poly(A) mRNA Magnetic Isolation Module and libraries were prepared using NEBNext Ultra II Directional RNA Library Prep Kit for Illumina according to the manufacturer's protocol. All libraries were normalized and pooled for paired-end 150bp sequencing with a single lane of an SP flowcell of Illumina NovaSeq 6000. Fastq files containing sequencing reads generated from paired-end RNA sequencing were analyzed using nf-core/rnaseq pipeline version 2.0 (Ewels et al., 2020) to determine read counts by featureCounts (Liao et al., 2014), which were mapped to GRCm38 genome database by STAR aligner (ver. 2.6.1d) (Dobin et al., 2013). Reads were then further analyzed using OmicsBox software (version 1.4.11) for DE analysis, which employs the package EdgeR (ver. 3.11) (Robinson et al., 2010). Reads were normalized using the Trimmed Mean of M-values (TMM) normalization method and a cut-off of at least 0.2 counts per million (CPM) in two samples was selected. Differentially expressed genes (DEGs) with a P value of <0.05 in the exact test, which is based on the quantile-adjusted conditional maximum likelihood (qCML) methods, were used for further analysis. Pathway analyses were performed using Qiagen Ingenuity Pathway Analysis software (ver. 01-19-02). The *Syt2* variant partition coverage and read density analyses were performed using Strand NGS (https://www.strand-ngs.com).

Genomic qPCR

For qPCR, genomic DNA was extracted from mouse hippocampi using NucleoSpin® Tissue (MACHEREY-NAGEL) following the manufacturer's protocol. Samples were treated with RNase A before column purification. Real-time PCR was performed using TB Green Premix Ex Taq II (Tli RNaseH Plus) (TAKARA) and ViiA7 Real-Time PCR system, Software v1.2 (Applied Biosystems) according to the manufacturer's protocol. Primer sequences are listed in Table S5.

Targeted Locus Amplification (TLA) analysis

Isolation of bone marrow cells was performed as described previously (Amend et al., 2016). Briefly, bone marrow cells were isolated by centrifugation at 10,000 xg from the femur and tibia of 4-month-old female CamiCre$^+$ mice. Cells were suspended in PBS, counted, resuspended in 5 x 10^6 cells/ml with Cell Banker1 (amsbio) and stored in −80C. Three vials containing 0.8 mL of the cell suspension each were sent

to commercially available TLA analysis service, Cergentis (https://www.cergentis.com/technology/tla-technology).

Behavioral analysis

Male CamiCre^{+} and WT mice were housed together, with two to five littermates (or mice with close birthdays) per cage after weaning. Mice (7–8 weeks of age) were acclimated to handling and the experimental room for at least three days before the start of an experiment. Mice underwent a battery of behavioral tests in the following order with at least one day between tests: open field, elevated plus maze, y-maze, light-dark transition, cued and contextual fear conditioning, and forced swim. Experimenters were blinded to the genotype during testing. All experiments were analyzed using an automated system from O'hara & Co. All software for analysis, which was based on the public domain program, ImageJ (https://imagej.nih.gov/nih-image/), was from O'hara & Co.

Open field test

Each subject was placed in the center of an open-field apparatus (50 × 50 × 33.3 cm; W x D x H) illuminated at 100 lux and allowed to move freely for 15 min. Distance travelled in the arena, trace of the movement, and time spent in the center were recorded and analyzed using Time OFCR software.

Elevated plus maze

The elevated plus maze (EP-3002) consists of two open arms and two closed arms (25 L x 5 W cm) extending from a central area (5 × 5 cm) and is elevated 50 cm from the ground. Mice were placed in the central area of the maze facing one of the open arms under illumination of 100 lux and allowed to move freely for 10 min. The number of entries into open or closed arms and the time spent in each arm were recorded and analyzed using Time EPC software.

Y-maze

Mice were placed at the end of one arm of a Y-shaped maze (YM-3002) with three matte gray PVC arms (3 × 40 × 12 cm; W x D x H) at a 120° angle from each other, illuminated at 50 lux for 10 min. Entry sequence into each arm and the total number of arm entries were recorded using Time YM software. Alternation is defined as entry into all three arms on consecutive choices. An entry occurs when all four limbs of the mouse are within the arm. The alternation score (%) was calculated using the following equation: $\frac{\#\ of\ alternations}{total\ arm\ entries-2} \times 100$.

Light-dark transition test

The apparatus consisted of a box (20 × 20 × 25 cm) divided into two compartments of equal size by a partition with a door: a white polyvinylchloride chamber illuminated at 500 lux and a black polyvinylchloride chamber without illumination. Mice were placed in the dark compartment and allowed to move freely with the door open for 15 min. The total number of transitions, time spent on each side, and latency to enter the light side were recorded and analyzed automatically using Time LD software.

Contextual and cued fear conditioning

Fear conditioning was conducted in a conditioning chamber (10 × 10 × 10 cm) surrounded by a sound-attenuating chamber. On day 1, mice were placed in the conditioning chamber (CL-3002L) for 120 s as habituation and then presented with 3 tone-shock pairs at 90 seconds intervals. The tone-shock pair consists of a tone (65-dB/10-kHz) for 30 seconds and a foot shock of 0.5mA during the last 2 s of the tone. Following the last tone-shock pair, mice were left in the chamber for 90 s. On day 2, mice were placed in the conditioning chamber without any tone-shock pairs for 360 s to test contextual learning. On day 3, mice were placed in a novel chamber (CLT-3002L) for 180 s and then presented with a tone for 180 s to test cued learning. Freezing responses were automatically recorded during each test and analyzed using Image FZC 2.22 sr2 software.

Forced swim test

Mice were placed in a Plexiglas cylinder (20 cm H x 11.4 cm D) filled with water (23–25°C) under 300 lux illumination. Duration of immobility (freezing) was recorded automatically during a 10 min test session using

the ImagePS/TS software. Percentage of immobility was calculated for the last 8 minutes. After testing, mice were removed and dried before being placed in their home cage.

QUANTIFICATION AND STATISTICAL ANALYSIS

Statistical analyses in this work employed unpaired two-tailed Student's *t* tests, two-tailed Welch's *t* tests, two-tailed paired *t* tests, or a two-way ANOVA with Geisser-Greenhouse correction, where appropriate, using GraphPad Prism 9. Details of each statistical test are described in the figure legend. A *P* value of <0.05 was considered statistically significant unless noted otherwise.